 CMES, vol.49, no.1, pp.23-45, 2009

A Rate-Dependent Damage/Decohesion Model for Simulating Glass Fragmentation under Impact using the Material Point Method

Luming Shen[1]

Abstract: A bifurcation-based simulation procedure is proposed in this paper to explore the transition from localization to decohesion involved in the glass fragmentation under impact loading. In the proposed procedure, the onset and orientation of discontinuous failure of glass is identified from the bifurcation analysis based on a rate-dependent tensile damage model. The material point method, which does not involve fixed mesh connectivity, is employed to accommodate the multi-scale discontinuities associated with the fragmentation of glass using a simple interface treatment. A parametric study has been conducted to demonstrate the effects of specimen size and impact velocity on the evolution of glass failure under impact loading. The preliminary results obtained in this numerical study provide a better understanding of the physics behind glass fragmentation under impact loading.

Keywords: damage, decohesion, bifurcation, glass, fragmentation, material point method, impact.

1 Introduction

Terrorist bomb attacks and threats are on the rise all over the world. It is estimated that most injuries from bomb blasts can be attributed to airborne sharp glass fragments. Hence, it is very important for us to thoroughly understand the failure mechanism of glass under impact/blast loading in order to develop better blast-resistant transparency and mitigate the injury or death due to flying glass fragments. Dynamic failure of glass has been the focus of considerable theoretical, experimental and numerical investigations [Brar, Bless and Rosenberg (1991); Bourne, Rosenberg and Field (1995); Kanel, Razorenov and Fortov (1992); Kanel, Razorenov, Savinykh, Rajendran and Chen (2005); Wei and Dharani (2005); among others].

[1] School of Civil Engineering, University of Sydney, NSW 2006, Australia. Tel: +61-2-93512126; Fax: +61-2-93513343; Email: L.Shen@usyd.edu.au.

Experimental investigations such as full-scale explosion tests tend to be expensive, environmentally unfriendly and time consuming. On the contrary numerical simulation of glass failure under blast/impact loading would be a lot more economical, more environmentally friendly and less time consuming.

Owing to the rapid improvement in computer hardware and computational tools, numerical modelling and simulation of complex impact, penetration, and fragmentation problems has become possible [Anderson and Bodner (1988); Chen, Feng, Xin and Shen (2003), Chen, Shen, Kanel and Razorenov (2001); Zukas (1990)]. The computational codes used for the simulation of these problems can be classified as Eulerian or Lagrangian with advantages and disadvantages depending upon the framework used [Anderson and Bodner (1988)]. So far, many simulations of impact, penetration, brittle failure, and fragmentation have tended to use Lagrangian approaches [Camacho and Ortiz (1988); Johnson, Stryk, Beissel and Holmquist (2001)], such as finite element method, with special techniques for simulating fracture and failure. However, the issues of considerable complexity in handling contact, mesh entanglement due to material fragmentation, and difficulties encountered while solving large deformation fluid-structure interaction problems have led to the exploration of alternative approaches. As one of the innovative mesh-free particle methods, the material point method (MPM) uses Lagrangian particles embedded in a background Eulerian grid. Particles interact via the background computational grid with other particles in the same body, with particles in other solid bodies, and with particles in fluids if involved. Thus, these three issues mentioned in the context of conventional mesh-based methods could be circumvented.

To explicitly simulate the fracture and/or fragmentation of materials, a rigorous cohesive/fracture model is essential. To date, several kinds of cohesive/fracture models have been proposed for simulating brittle failure, as discussed by the representative papers [Klein, Foulk, Chen, Wimmer and Gao (2000); Le, Mai-Duy, Tran-Cong and Baker (2008); Schreyer, Sulsky and Zhou (1999); Xu and Needleman (1994); Zhang and Chen (2008)]. To achieve computational efficiency, however, in these studies the location and orientation of decohesion/fracture were either predefined, mesh-dependent or based on the maximum tensile stress (strain) without performing a discontinuous bifurcation analysis. As can be seen from Fig. 1, discontinuous bifurcation can occur before, at or after the peak state, depending on the continuum tangent stiffness tensor and stress state [Chen, Shen, Mai, and Shen (2005); Shen and Chen (2005a); (2005b)]. It is therefore not rigorous to distribute arbitrarily cohesive surfaces in a computational mesh and initiate decohesion at a predefined state. Based on recent studies [Chen, Shen, Mai, and Shen (2005); Shen, Liu and Chen (2001)], in fact, the discontinuous bifurcation analysis could be performed without too much computational cost when an associated von Mises

elasto-plasticity model or a rate-dependent damage model is used.

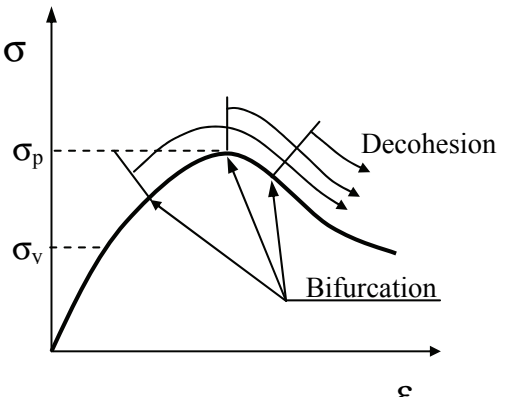

Figure 1: Discontinuous bifurcation might occur before, at or after the limit state.

In this paper, a rate-dependent tensile damage/decohesion model is proposed for modelling glass fragmentation within the framework of the MPM. In the proposed model, bifurcation analysis is performed to identify the initiation and orientation of discontinuous failure. To demonstrate the potential of the proposed rate-dependent tensile damage/decohesion model, the failure of a circular glass plate under impact of a high velocity steel cylinder is simulated using the MPM.

The remaining sections of the paper are arranged as follows. A brief description of the MPM is presented in Section 2, which is followed by the description of the proposed constitutive models for glass and steel in Section 3. A case study of steel cylinder impacting on circular glass plate is performed to evaluate the proposed approach and the simulation results are discussed in Section 4. The conclusions and future work are given in the last section.

2 The material point method

As indicated by Belytschko, Krongauz, Organ, Fleming, and Krysl (1996), Klein, Foulk, Chen, Wimmer and Gao (2000), Atluri (2004), Atluri, Han, and Rajendran (2004), Li and Atluri (2008) and others for model-based simulation with cohesive/fracture formulations, the meshfree particle methods are uniquely suitable for those problems such as localized large deformations, propagation of cracks, separation of continuum and fragmentation, for which the conventional mesh-based methods such as finite element are handicapped. In fact, the key difference among different spatial discretization methods is the way how the gradient and divergence

terms are calculated. Because the meshfree particle methods do not use rigid mesh connectivity as compared with the mesh-based methods the interpolation in the moving domain of influence is the common feature of the meshfree particle methods.

As one of the innovative spatial discretization methods, the MPM is an extension to solid mechanics problems of a hydrodynamics code called FLIP that, in turn, evolved from the Particle-in-Cell Method dating back to the pioneering work of Harlow (1964). The motivation of developing the MPM was to simulate those challenging problems such as impact/contact, penetration and machine processing with history-dependent internal state variables, as shown in the early publications about the MPM [Sulsky, Chen and Schreyer (1994); Sulsky, Zhou and Schreyer (1995)]. The essential idea of the MPM is to take advantage of both the Eulerian and Lagrangian methods while avoiding the shortcomings of each. In comparison with the other meshless methods, the MPM appears to be less complex with a cost factor of at most twice that associated with the use of corresponding finite elements [Chen, Hu, Shen, Xin and Brannon (2002)]. In addition, the use of the single-valued mapping functions in the MPM results in a natural no-slip contact/impact scheme without invoking master/slave nodes so that no inter-penetration would occur in multi-body interaction problems. Recently, much research has been conducted to improve the spatial discretization methodology proposed in the original MPM such that the MPM could be applied to more engineering problems of current interests [Bardenhagen and Kober (2004); Guo and Nairn (2006); Hu and Chen (2006); Nairn (2003); Shen and Chen (2005a); Wallstedt and Guilkey (2007); among others]. To illustrate how the transition from continuous to discontinuous failure modes in the glass fragmentation could be simulated with the proposed numerical procedure, the framework of the MPM is briefly outlined as follows.

The MPM discretizes a continuum body with the use of a finite set of N_p material points in the original configuration that are tracked throughout the deformation process. Let $\mathbf{x}_p^t$ ($p = 1, 2, \ldots, N_p$) denote the current position of material point p at time t. Each material point at time t has an associated mass M_p, density ρ_p^t, velocity $\mathbf{v}_p^t$, Cauchy stress tensor $\boldsymbol{\sigma}_p^t$, strain $\boldsymbol{\varepsilon}_p^t$, and any other internal state variables necessary for constitutive modeling. Thus, these material points provide a Lagrangian description of the continuum body. Since each material point contains a fixed amount of mass unless the material point is further divided into smaller points for multi-scale modeling, the conservation of mass is automatically satisfied. At each time step, the information from the material points is mapped to a background computational mesh (grid). This mesh covers the computational domain of interest, and is chosen for computational convenience. After the information is mapped from the material points to the mesh nodes, the discrete equations of the conservation of

momentum are solved on the mesh nodes. The nodal solutions are then mapped back to update material points, which completes the computational cycle within one time step.

Based on the standard procedure used in the finite element method, the weak form of the conservation of momentum is found to be

$$\int_{\Omega} \rho \mathbf{w} \cdot \mathbf{a} d\Omega = -\int_{\Omega} \rho \boldsymbol{\sigma}^s : \nabla \mathbf{w} d\Omega + \int_{S^c} \rho \mathbf{c}^s \cdot \mathbf{w} dS + \int_{\Omega} \rho \mathbf{w} \cdot \mathbf{b} d\Omega \tag{1}$$

in which w denotes the test function, a is acceleration, $\boldsymbol{\sigma}^s$ is specific stress (i.e., stress divided by mass density), $\mathbf{c}^s$ is specific traction vector (i.e., traction divided by mass density), $\mathbf{b}$ is specific body force, Ω is current configuration of the continuum, and S^c is that part of the boundary with a prescribed traction. The test function w is assumed to be zero on the boundary with a prescribed displacement. Since the whole continuum body is described with the use of a finite set of material points (mass elements), the mass density term can be written as

$$\rho(\mathbf{x},t) = \sum_{p=1}^{N_p} M_p \delta\left(\mathbf{x} - \mathbf{x}_p^t\right) \tag{2}$$

where δ is the Dirac delta function with dimension of the inverse of volume. The substitution of Eq. (2) into Eq. (1) converts the integrals to the sums of quantities evaluated at the material points; namely

$$\sum_{p=1}^{N_p} M_p \left[\mathbf{w}\left(\mathbf{x}_p^t,t\right) \cdot \mathbf{a}\left(\mathbf{x}_p^t,t\right)\right] = \sum_{p=1}^{N_p} M_p \left[-\boldsymbol{\sigma}^s\left(\mathbf{x}_p^t,t\right) : \nabla \mathbf{w}|_{\mathbf{x}_p^t}\right.$$

$$\left. + \mathbf{w}\left(\mathbf{x}_p^t,t\right) \cdot \mathbf{c}^s\left(\mathbf{x}_p^t,t\right) h^{-1} + \mathbf{w}\left(\mathbf{x}_p^t,t\right) \cdot \mathbf{b}\left(\mathbf{x}_p^t,t\right)\right] \tag{3}$$

with h being the thickness of the boundary layer. As can be observed from Eq. (3), the interactions among different material points are reflected only through the gradient terms which necessitate the use of a background mesh. Different constitutive models (continuum or discrete) can be applied to the material points for given total strains. Complete decohesion would occur if the material strength is totally lost. In other words, a material point would be separated from the original continuum body if there is no internal interaction between the point (with zero strength) and the body (with nonzero strength). Because there is no fixed mesh connectivity between the material points and the background mesh in the MPM, localization and the transition from continuous to discontinuous failure modes could be simulated without the difficulties associated with remeshing.

3 Constitutive models

3.1 From continuous failure to decohesion

Since the material failure is an evolving process that involves jumps in certain field variables, the discontinuous bifurcation analysis is performed based on the jump forms of conservation laws [Chen (1996)]. With the jumps in the kinematic field variables of a continuum body, the evolution of material failure process can be divided into diffuse failure ($\mathbf{v}_1 = \mathbf{v}_2$ and $\dot{\boldsymbol{\varepsilon}}_1 = \dot{\boldsymbol{\varepsilon}}_2$), localized failure ($\mathbf{v}_1 = \mathbf{v}_2$ and $\dot{\boldsymbol{\varepsilon}}_1 \neq \dot{\boldsymbol{\varepsilon}}_2$) and discrete failure ($\mathbf{v}_1 \neq \mathbf{v}_2$ and $\dot{\boldsymbol{\varepsilon}}_1 \neq \dot{\boldsymbol{\varepsilon}}_2$) with $\mathbf{v}_1$ and $\mathbf{v}_2$ being the velocity vectors and $\dot{\boldsymbol{\varepsilon}}_1$ and $\dot{\boldsymbol{\varepsilon}}_2$ being the total strain rates on the side 1 and 2 of a moving surface of discontinuity, respectively. As can be seen, the jump degree in the kinematic field variables identifies the initiation of different failure states at different scales [Bazant and Chen (1997)]. The transition from continuous to discontinuous failure states is characterized by the condition of localized failure that can be determined via the discontinuous bifurcation analysis of the acoustic tensor [Iordache and Willam (1998); Ottosen and Runesson (1991) among others]. Because there is a jump in the strain rate for localized failure, it is reasonable to claim that a corresponding jump must exist in mass density. The jump in mass density results in a moving, instead of a stationary, surface of discontinuity governed by the jump forms of conservation laws [Chen (1996)]. Without explicitly tracing each individual surface of discontinuity, a computational efficient and mathematically rigorous approach is proposed in this paper to describe the transition from continuous to discontinuous failure for glass and steel.

Since glass is brittle and steel is ductile, different constitutive models need to be developed for glass and steel. To account for the facts that the compressive strength of glass is much higher than the tensile strength and its strength varies as a function of loading rate, an elastic-perfectly plastic Drucker-Prager model will be used in the compressive regime of glass, while a rate-dependent damage model will be used before the localization and a bifurcation-based decohesion model is adopted after the localization for glass under tensile loading. For steel, an associated von Mises model with a linear hardening and softening law is used before the localization. A bifurcation-based decohesion model is then applied to steel once the localization has occurred. The formulations of the constitutive models for glass and steel will be discussed in Sections 3.2 and 3.3, respectively.

3.2 Constitutive models for glass

In this study, a combined rate-dependent local damage/plasticity model developed to study the stress-wave-induced fracturing for brittle materials [Taylor, Chen and Kuszmaul (1986); Chen, Hu and Chen (2001); Hu and Chen (2006)] will be adopted

to model the glass responses under dynamic loading. Within the loading regime of the model, an isotropic elasticity tensor governs the elastic material behavior; a scalar measure of continuum damage is active through the rate-dependent degradation of the elasticity tensor if the confining pressure P>0 (tensile regime); and an elastic-perfectly plastic Drucker-Prager model is used if P<0 (compressive regime). A decohesion model is activated once the initiation of the discontinuous failure is identified through bifurcation analysis for glass under tension. It is assumed that no additional damage would occur as long as decohesion evolves in the material element. Decohesion will not be introduced for glass under compression.

The stress-strain relation for the rate-dependent tensile damage model is given by

$$\boldsymbol{\sigma} = \mathbf{E}^{ed} : \boldsymbol{\varepsilon} \tag{4}$$

where $\boldsymbol{\sigma}$ denotes a stress tensor, $\boldsymbol{\varepsilon}$ a total strain tensor, and $\mathbf{E}^{ed}$ a secant elastodamage stiffness tensor. The rate-dependent elastodamage stiffness tensor is updated with the evolution of the bulk modulus K and Poisson's ratio υ, which can be described as below.

$$\bar{K} = (1-D)\,K \tag{5}$$

$$\bar{\upsilon} = \upsilon\left(1 - \frac{16}{9}\rho_d\right) \tag{6}$$

$$\rho_d = 2.5k\left(\frac{K_{IC}}{\rho c \dot{\varepsilon}_{\max}}\right)^2 \varepsilon_v^m \tag{7}$$

$$D = 16\rho_d\left(1-\bar{\upsilon}^2\right)/\left[9\left(1-2\bar{\upsilon}\right)\right] \tag{8}$$

where ρ_d is a crack-density parameter, K_{IC} the fracture toughness, ε_v the mean volumetric strain, $\dot{\varepsilon}_{\max}$ the maximum volumetric strain rate experienced by the material at fracture, c the uniaxial wave speed, ρ the volume density of materials, $\bar{K}$ the bulk modulus of damaged materials, respectively, $\bar{\upsilon}$ the Poisson's ratio of the damaged materials, respectively, k and m two model parameters, and D a single damage parameter. To perform bifurcation analysis, a continuum tangent stiffness tensor is needed. The rate form of stress-strain relation for the rate-dependent tensile damage model takes the form of

$$\dot{\boldsymbol{\sigma}} = \mathbf{T}^{ed} : \dot{\boldsymbol{\varepsilon}} \tag{9}$$

where $\mathbf{T}^{ed}$ is the tangent elastodamage stiffness tensor. A bifurcation analysis of the acoustic tensor can be performed based on Eq. (9) to identify the transition from continuous to discontinuous failure modes, and the corresponding orientation

of failure surface. As demonstrated in the previous work [Chen, Deng and Chen (2001)], the failure angle is rate-independent although the failure strain is rate-dependent for the proposed tensile damage model.

Based on the previous research on decohesion models [Shen, Liu and Chen (2001), Chen and Fang (2001); Chen, Shen, Mai and Shen (2005)], a bifurcation-based rate-dependent decohesion model is formulated to predict the initiation and orientation of discontinuous failure. As illustrated in Fig. 2 for two-dimensional cases, $\mathbf{n}$ and $\mathbf{t}$ denote the unit normal and tangent vectors to the cohesive surface, respectively, after bifurcation occurs. The normal vector is related to the critical failure angle through $\mathbf{n} = (-\sin\theta^{cr}\mathbf{i}, \cos\theta^{cr}\mathbf{j})$, with $\mathbf{i}$ and $\mathbf{j}$ denoting the unit vector along the x- and y-axis, respectively.

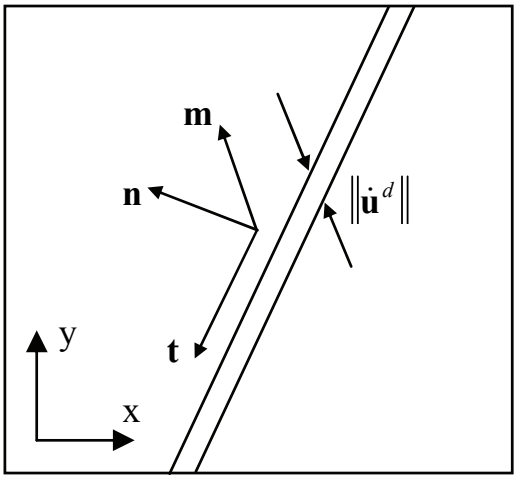

Figure 2: A 2-dimensional element with decohesion.

To determine the discrete constitutive relation between the traction $\boldsymbol{\tau}$ and decohesion $\mathbf{u}^d$, the following equations, which satisfy the thermodynamic restrictions, can be developed for a given total strain rate $\dot{\boldsymbol{\varepsilon}}$ [Schreyer, Sulsky, Zhou (1999); Chen, Shen, Mai and Shen (2005)]:

$$\dot{\boldsymbol{\sigma}} = \mathbf{E} : \left(\dot{\boldsymbol{\varepsilon}} - \dot{\boldsymbol{\varepsilon}}^d\right) \tag{10}$$

$$\dot{\tau} = \dot{\boldsymbol{\sigma}} \cdot \mathbf{n} \tag{11}$$

$$\dot{\boldsymbol{\varepsilon}}^d = \dot{\lambda}^d \left(\mathbf{n} \otimes \mathbf{m} + \mathbf{m} \otimes \mathbf{n}\right) / \left(2L_e\right) \tag{12}$$

$$f^d = \tau^e - U_0 \left[1 - \left(\lambda^d\right)^q\right] = 0 \tag{13}$$

$$\dot{\mathbf{u}}^d = \dot{\lambda}^d \mathbf{m} \tag{14}$$

where $\dot{\lambda}^d$ is a dimensionless monotonically increasing variable characterizing the evolution of decohesion, L_e is the effective length representing the ratio of the volume to the area of the decohesion within a material element, and U_0 is the reference surface energy defined as the product of the reference decohesion scalar $\bar{u}_0$ and corresponding traction $\bar{\tau}_0$. The effective traction τ^e takes the form of

$$\tau^e = \tau \cdot \mathbf{m} = \bar{u}_0 \sqrt{\tau \cdot \mathbf{T}_d \cdot \tau} \tag{15}$$

with an associated evolution equation, namely

$$\mathbf{m} = \bar{u}_0 \left(\mathbf{T}_d \cdot \tau\right) / \left(\sqrt{\tau \cdot \mathbf{T}_d \cdot \tau}\right). \tag{16}$$

The components of the positive definite tensor of material parameters, $\mathbf{T}_d$, with respect to the **n – t** basis are given by

$$[T_d] = \bar{\tau}_0^2 \begin{bmatrix} \frac{1}{\tau_{np}^2} & 0 \\ 0 & \frac{1}{\tau_{tp}^2} \end{bmatrix} \tag{17}$$

At the initiation of decohesion ($\lambda^d = 0$), it follows from Eqs. (13), (15) and (17) that

$$\frac{\tau_{nb}^2}{\tau_{np}^2} + \frac{\tau_{tb}^2}{\tau_{tp}^2} = 1 \tag{18}$$

where the normal and tangential tractions, τ_{nb} and τ_{tb}, are obtained from the discontinuous bifurcation analysis. By letting $C_m = \tau_{tp}/\tau_{np}$, different failure modes can be simulated utilizing different values of C_m and Eq. (18). For example, mode I failure dominates if $C_m = 100$, while mode II failure dominates if $C_m = 0.01$. Mixed failure modes could be simulated by using $C_m = 1$, depending on the critical state. Well-designed experiments are required to calibrate the value of C_m. The reference traction values, τ_{np} and τ_{tp}, can be found from Eq. (18) evaluated at the initiation of bifurcation for a given C_m. As can be seen from the above formulations, the discrete model parameters to be determined from the experiments are U_0, q and C_m if the choice of $\tau_{np} = \bar{\tau}_0$ is made. The relation between the traction and decohesion can be adjusted by changing the value of q, as illustrated in Fig. 3 with a linear relation being obtained if $q = 1$.

A standard elastic-perfectly plastic Drucker-Prager model is adopted for glass under compressive loading regime. The yield surface takes the form of

$$f(\boldsymbol{\sigma}) = \bar{\sigma}^2 - (\sigma_y + \beta P)^2 = 0 \tag{19}$$

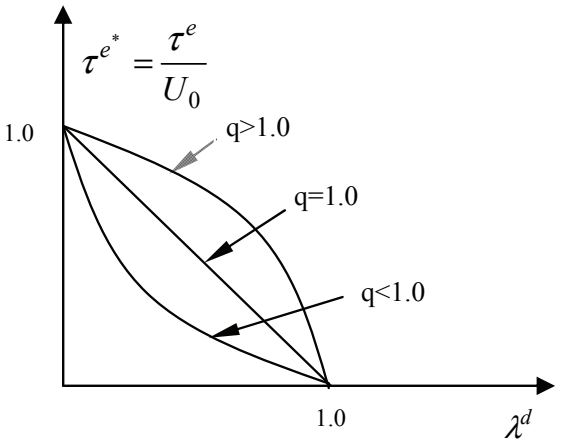

Figure 3: The relationship between effective traction and effective decohesion.

in which $\bar{\sigma} = \sqrt{\frac{3}{2}\boldsymbol{\sigma}^d : \boldsymbol{\sigma}^d}$ is the effective stress with $\boldsymbol{\sigma}^d$ being the deviatoric stress tensor, $P = -\frac{1}{3}\sigma_{ii}$ the mean pressure, and β a material constant.

3.3 Constitutive models for steel

Following the previous work on the bifurcation-based decohesion model for simulating tungsten film delaminating from silicon substrate [Chen, Shen, Mai and Shen (2005)], an associated von Mises model with a linear hardening and softening law is applied to steel before the localization. The model consists of the following equations:

$$d\boldsymbol{\sigma} = \mathbf{E} : (d\boldsymbol{\varepsilon} - d\boldsymbol{\varepsilon}^p) \tag{20}$$

$$f(\boldsymbol{\sigma}, I) = \begin{cases} \bar{\sigma}^2 - (\sigma_y + E_h I)^2 = 0 & 0 \le I < I_p \\ \bar{\sigma}^2 - [\sigma_p - E_s (I - I_p)]^2 = 0 & I \ge I_p \end{cases} \tag{21}$$

$$d\boldsymbol{\varepsilon}^p = d\phi \frac{\partial f}{\partial \boldsymbol{\sigma}} \tag{22}$$

$$dI = d\phi = (d\boldsymbol{\varepsilon}^p : d\boldsymbol{\varepsilon}^p)^{\frac{1}{2}} \tag{23}$$

in which $\mathbf{E}$ denotes linear isotropic elasticity tensor, $\boldsymbol{\varepsilon}^p$ inelastic strain tensor, $f(\boldsymbol{\sigma}, I) = 0$ inelastic surface with I representing the internal state variable,I_p the internal state variable corresponding to the peak state, σ_y the yield strength, σ_p the peak strength, E_h the hardening modulus and E_s the softening modulus, and ϕ

a parameter characterizing the loading process. Either an incremental-iterative or one-step solution scheme could be employed to integrate the above set of constitutive equations, depending on the error tolerance.

The continuum tangent stiffness tensor corresponding to the above von Mises model can be found to be

$$\mathbf{T} = \mathbf{E} - H\boldsymbol{\sigma}^d \otimes \boldsymbol{\sigma}^d \tag{24}$$

where $H = 4G^2 / \left[\left(2G - \frac{1}{N}\frac{\partial f}{\partial I} \right) \left(\boldsymbol{\sigma}^d : \boldsymbol{\sigma}^d \right) \right]$ is used with $N = \sqrt{\frac{\partial f}{\partial \boldsymbol{\sigma}} : \frac{\partial f}{\partial \boldsymbol{\sigma}}}$ and with G being shear modulus. The discontinuous bifurcation occurs when H reaches the critical state, H^{cr}, that is defined by

$$H^{cr} = \left(G^2 + 3KG \right) / \left[3G \left(\sigma_0 - \sigma_c \right)^2 + \left(G + 3K \right) r^2 \right] \tag{25}$$

in which K is bulk modulus, $\sigma_o = \left(\sigma_1 + \sigma_2 + \sigma_3 \right) / 3$, $\sigma_c = 0.5 \left(\sigma_1 + \sigma_3 \right)$, and $r = 0.5 \left(\sigma_1 - \sigma_3 \right)$, with σ_1 and σ_3 being the maximum and minimum principal stress, respectively. The critical failure angle, θ^{cr}, is given by

$$\theta^{cr} = \pm \arctan \sqrt{\frac{3G \left(\sigma_c - \sigma_0 \right) - \left(G + 3K \right) r}{3G \left(\sigma_0 - \sigma_c \right) - \left(G + 3K \right) r}} \tag{26}$$

As can be seen, the initiation and orientation of localized failure depend on the material properties and stress state. Because the critical state has been identified via the closed-form solutions, the same procedure described in Eqs. (10)-(18) can be used to couple the bifurcation analysis with the discrete constitutive model and to predict the decohesion of steel.

4 Demonstration

To demonstrate the potential of the proposed tensile damage model and bifurcation-based decohesion model for simulating glass fragmentation, numerical simulations of a steel cylinder impacting on a circular glass plate are performed by using the MPM. The configuration of the axisymmetrical problem is shown in Fig. 4. The glass plate has a thickness of 5 mm and a radius of R with its perimeter being fixed. The steel cylinder has a height of 50 mm and a radius of 5 mm. The initial separation between the impactor and the plate is 3 mm. The steel cylinder impacts at the center of the glass plate in the normal direction.

Before the discontinuous bifurcation occurs, the associated von Mises elastoplasticity model with a linear hardening/softening function is used for steel, for which Young's modulus E = 195 GPa, Poisson's ratio υ = 0.25, mass density ρ = 7,800

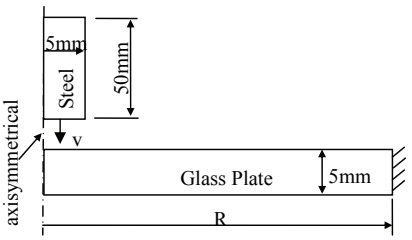

Figure 4: Configuration of the axisymmetrical problem.

kg/m^3, hardening modulus E_h = 9.6 GPa, and softening modulus E_s = 9.6 GPa are assigned for a parametric study. In addition, yield strength σ_y = 359 MPa and peak strength σ_p = 484 MPa are adopted. Note that no dynamic effect on the mechanical properties of steel is considered since the focus of this study is on the glass failure. After bifurcation occurs, the discrete constitutive model is active with $\bar{u}_0 = 1.60 \times 10^{-9} m$, q = 1.0, and C_m = 1.0.

For the glass, the model parameters are assigned with the following values: Young's modulus E = 72 GPa, Poisson's ratio υ = 0.25, mass density ρ = 2,500 kg/m^3, fracture toughness $K_{IC} = 0.83 MPa\sqrt{m}$, yield strength σ_y = 43 MPa, the Drucker-Prager model parameter β = 1.8, the damage model parameters k = 5.0x10^{26} m^{-3} and m = 6, and the decohesion model parameters $\bar{u}_0 = 5.0 \times 10^{-6} m$, q = 1.0, and C_m = 50.0.

In the MPM, the computational grid consists of square cells with each side being 1.0 mm long. Initially, one material point per cell is used to discretize both steel and glass. With the evolution of localization and decohesion, the number of material points per cell would change but the cell size is fixed. An explicit time integrator is adopted with time step of 0.2 μs.

To study the specimen size and loading rate effects on the failure mechanism of glass plate, numerical simulations of steel cylinder impacting on three different glass plates (R= 200 mm, 400 mm and 800 mm) at three different velocities (v = 200 m/s, 400 m/s and 800 m/s) are performed. Fig. 5 shows the snapshots of a steel cylinder impacting on a glass plate with R = 200 mm at a velocity of v = 200 m/s. Note that time t is set to be zero at the moment when the steel cylinder first time touches the glass plate. As can be seen from the figures, no fragmentation occurs at time t = 50 μs. Severe fragmentations first appear at the position about 30 mm from the impact center around time t = 100 μs. When the stress wave reaches the fixed end and is reflected back by the fixed boundary, the stress magnitude is doubled, which results in severe glass fragmentation near the end at time t = 150 μs. As the

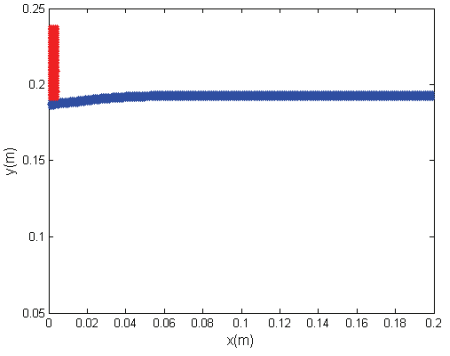

a). $t = 50$ µs

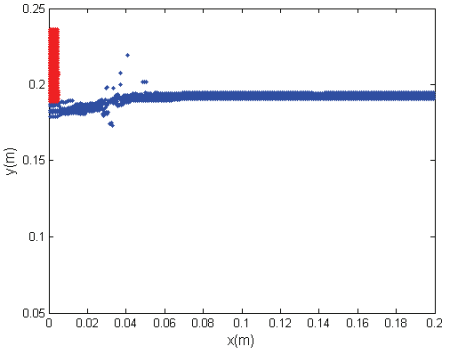

b). $t = 100$ µs

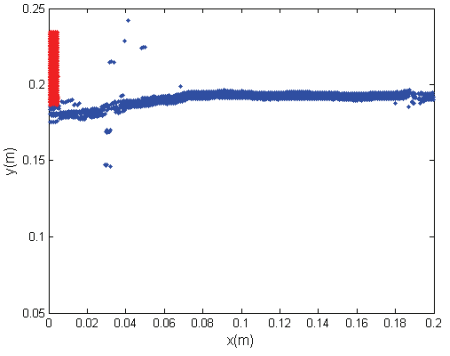

c). $t = 150$ µs

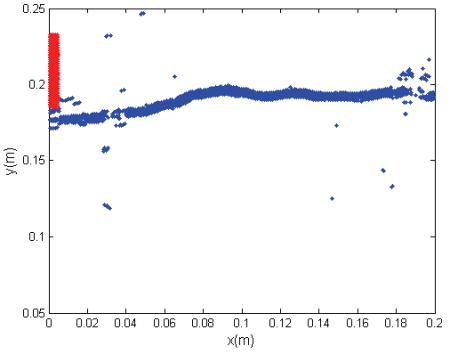

d). $t = 200$ µs

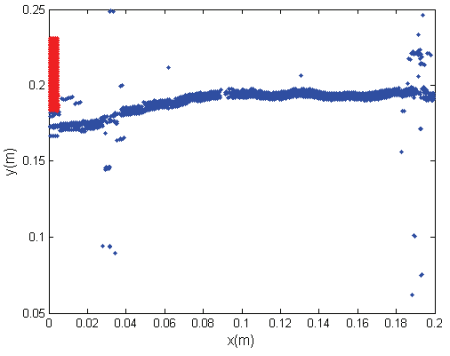

e). $t = 250$ µs

Figure 5: Snapshots of a steel cylinder impacting on a glass plate with R=200 mm at velocity of 200 m/s.

reflected stress wave travels further, the glass breaks at the distance 100 mm from the center.

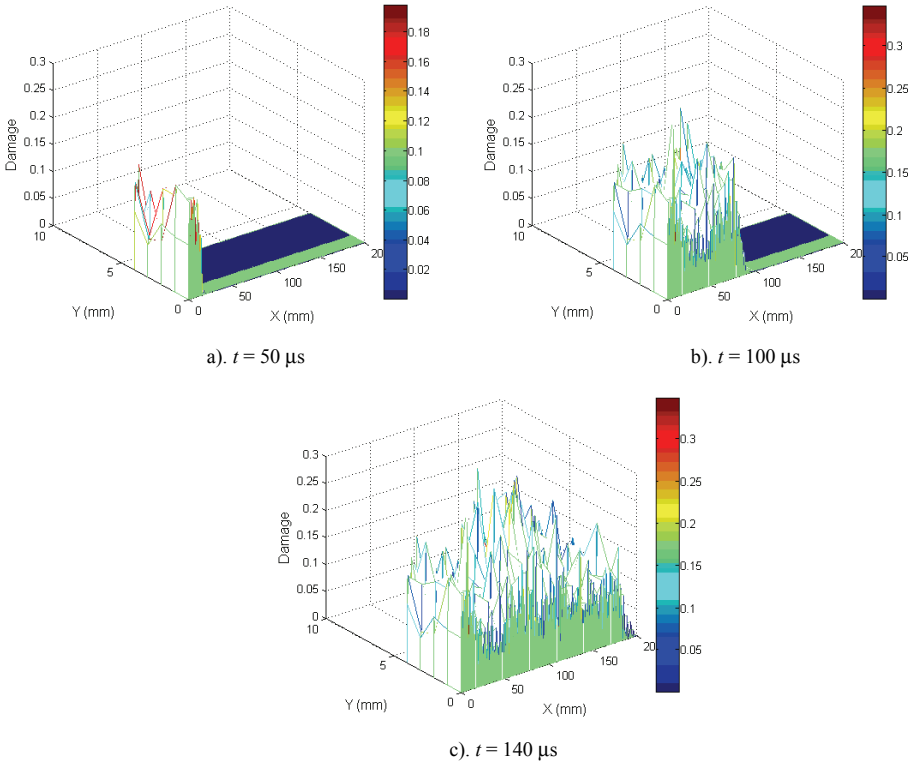

a). $t = 50$ μs b). $t = 100$ μs

c). $t = 140$ μs

Figure 6: Glass damage contours corresponding to Fig. 5.

The propagation of damage in glass plate with R = 200 mm impacted by a steel cylinder at velocity of 200 m/s is presented in Fig. 6. Note that damage occurs only in tensile loading regime and the evolution of damage ends after the localization has occurred. As can be seen from Fig. 6, the damage propagates from the impact center to the boundary as the stress wave travels, although the damage front travels at a velocity which is lower than that of stress wave. The propagation of the corresponding decohesion in glass plate is demonstrated in Fig. 7. The first decohesion occurs around time t = 70 us after impact and the largest decohesion is located about 25 mm away from the impact center, which is consistent with the failure patterns in Figure 5. The comparison between Fig. 6 and Fig. 7 indicates that the damage front is ahead of the fragmentation front since the localization only occurs when the damage reaches a certain level.

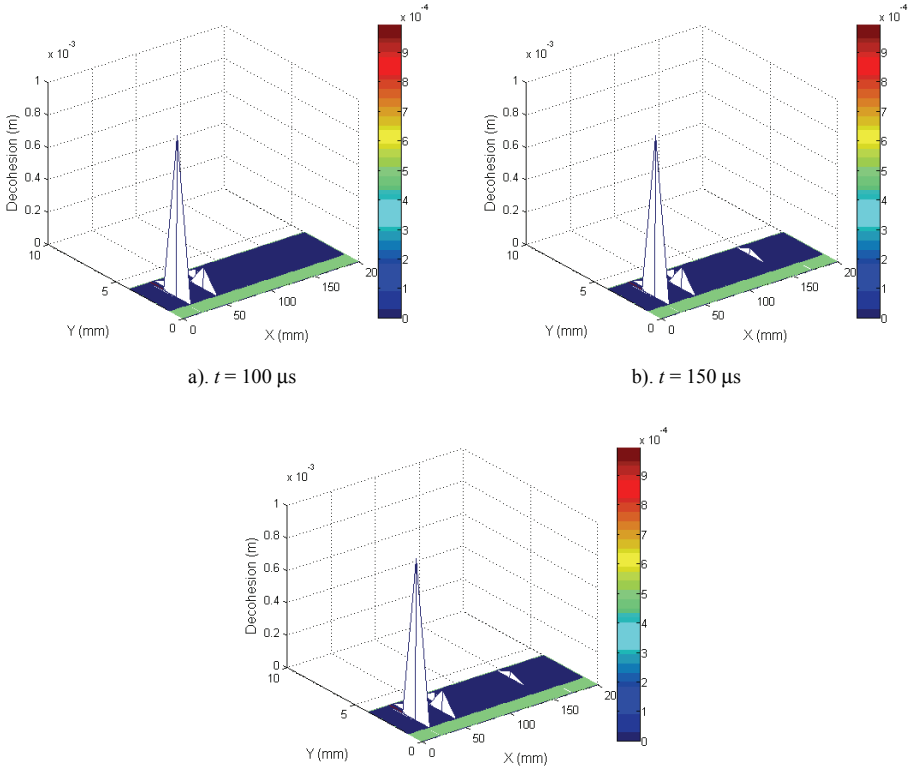

a). t = 100 μs

b). t = 150 μs

c). t = 200 μs

Figure 7: Glass decohesion contours corresponding to Fig. 5.

To investigate the effect of loading rate on the failure mechanism of glass, impact velocities of v = 400 m/s and v = 800 m/s are also used. Fig. 8 shows the snapshots of a steel cylinder impacting on a glass plate with R = 200 mm at an impact velocity of v = 800 m/s. As can be found from the figure, with a higher impact velocity the steel cylinder easily penetrates the glass plate. As the stress wave propagates, severe fragmentations occur at the position 50 mm from the impact center. Similarly, the glass breaks near the end due to the reflected stress wave.

The corresponding glass damage evolution is shown in Fig. 9. Compared with the damage evolution in Fig. 6, it seems that at a higher impact velocity, the damage propagates much faster. Since the velocity of stress wave is independent of the impact velocity, it seems that under a higher impact velocity more material points are under large tensile loading regime. The glass decohesion occurs right after

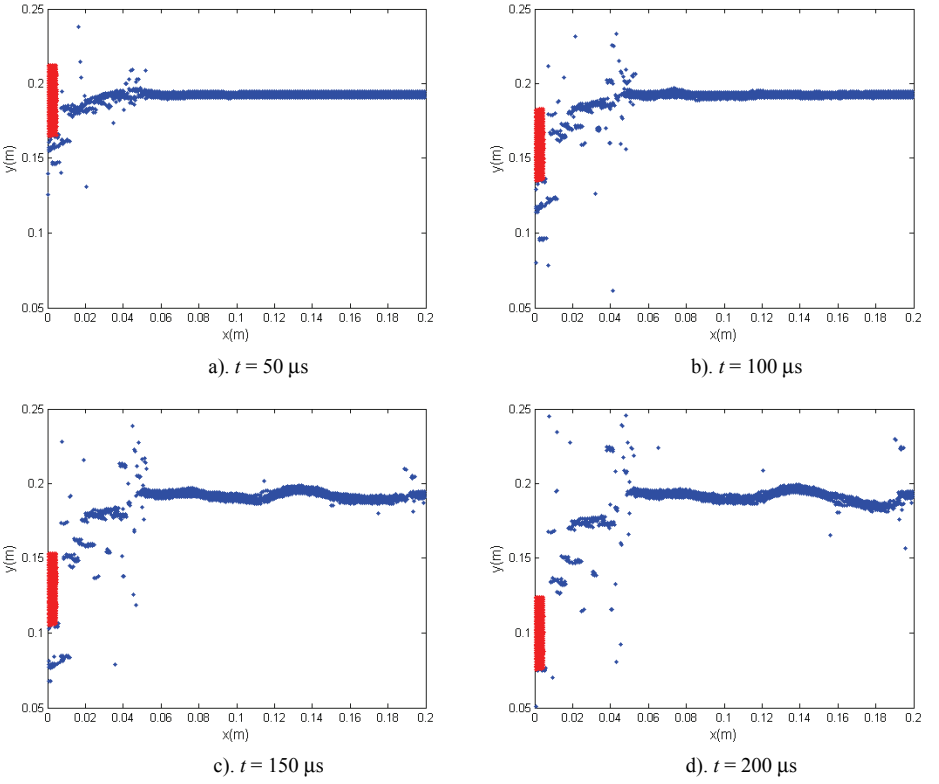

Figure 8: Snapshots of a steel cylinder impacting on a glass plate with R = 200 mm at velocity of 800 m/s.

impact as shown in Fig. 10(a). However, the propagation of the decohesion is slower, as demonstrated in Fig. 10, due to the quick penetration of the steel bar through the glass.

To study the size effect on the glass failure mechanism, glass plates with radii of 400 mm and 800 mm are also impacted by a steel cylinder at different velocities in the simulations. Fig. 11 presents the snapshots of a steel cylinder impacting on a glass plate with R = 400 mm at a velocity of v = 200 m/s. Again, no fragmentation occurs at time t = 50 μs. Severe fragmentations first appear at the place 50mm from the impact center at time t = 100 μs. At time t = 250 μs, the reflected stress wave cause the break of glass near the fixed end.

The evolution of damage in the glass plate with R = 400 mm impacted by a steel cylinder at velocity of 200 m/s is demonstrated in Fig. 12. Compared with the

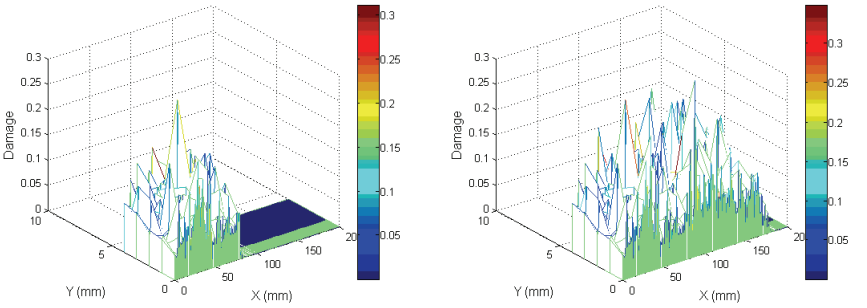

a). $t = 50$ µs b). $t = 100$ µs

Figure 9: Glass damage contours corresponding to Fig. 8.

damage evolution shown in Fig. 6, it seems that with a larger size glass plate, the damage propagates at a little bit higher velocity. This is because more material points are under tensile loading regime with a large glass plate under the same impact velocity.

5 Conclusions

A bifurcation-based simulation procedure has been proposed in this paper to explore the transition from localization to decohesion involved in the glass fragmentation under impact loading. In the proposed procedure, a rate-dependent tensile continuum damage/plasticity model is combined with a rate-dependent decohesion model via the bifurcation analysis so that the governing differential equations remain well posed for given boundary and/or initial data. Since no higher order terms in space are introduced into the stress–strain relations, the proposed procedure is sound in physics and efficient in computation.

In the simulation, the onset and orientation of discontinuous failure of glass is identified from the discontinuous bifurcation analysis based on a rate-dependent tensile damage model. Without explicitly treating individual surfaces of discontinuity, a discrete constitutive model is formulated based on the bifurcation analysis to predict the evolution of material failure as decohesion of continuum. The MPM is developed to accommodate the multi-scale discontinuities involved in the glass fragmentation with a simple interface treatment.

A parametric study has been conducted to demonstrate the effects of specimen size and strain rate on the evolution of failure patterns of glass under impact loading.

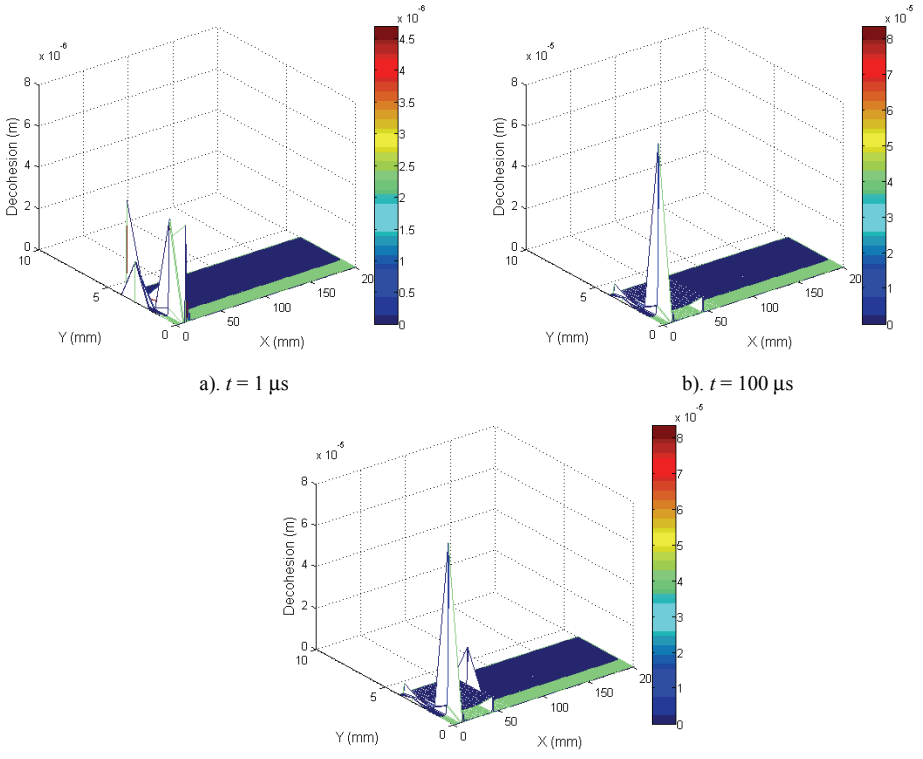

a). t = 1 μs

b). t = 100 μs

c). t = 200 μs

Figure 10: Glass decohesion contours corresponding to Fig. 8.

It appears from the simulation results that the damage propagates faster when the impact velocity is higher or the glass size is larger. The damage front is ahead of the fragmentation front as the localization only occurs when the damage reaches a certain level. The glass may break at the areas near both the impact center due to the direct impact loading and the fixed end due to the reflected stress wave.

Although well-designed experiments are required to explore the multi-scale failure mechanisms involved, the parametric study presented here provides a better understanding on the physics behind the glass fragmentation under impact loading. An integrated experimental, analytical and computational effort is required to further improve the proposed procedure for general applications.

Acknowledgement: The work was sponsored in part by the Australian Research Council (ARC) under Grant No. DP0772478. The support from NCI National

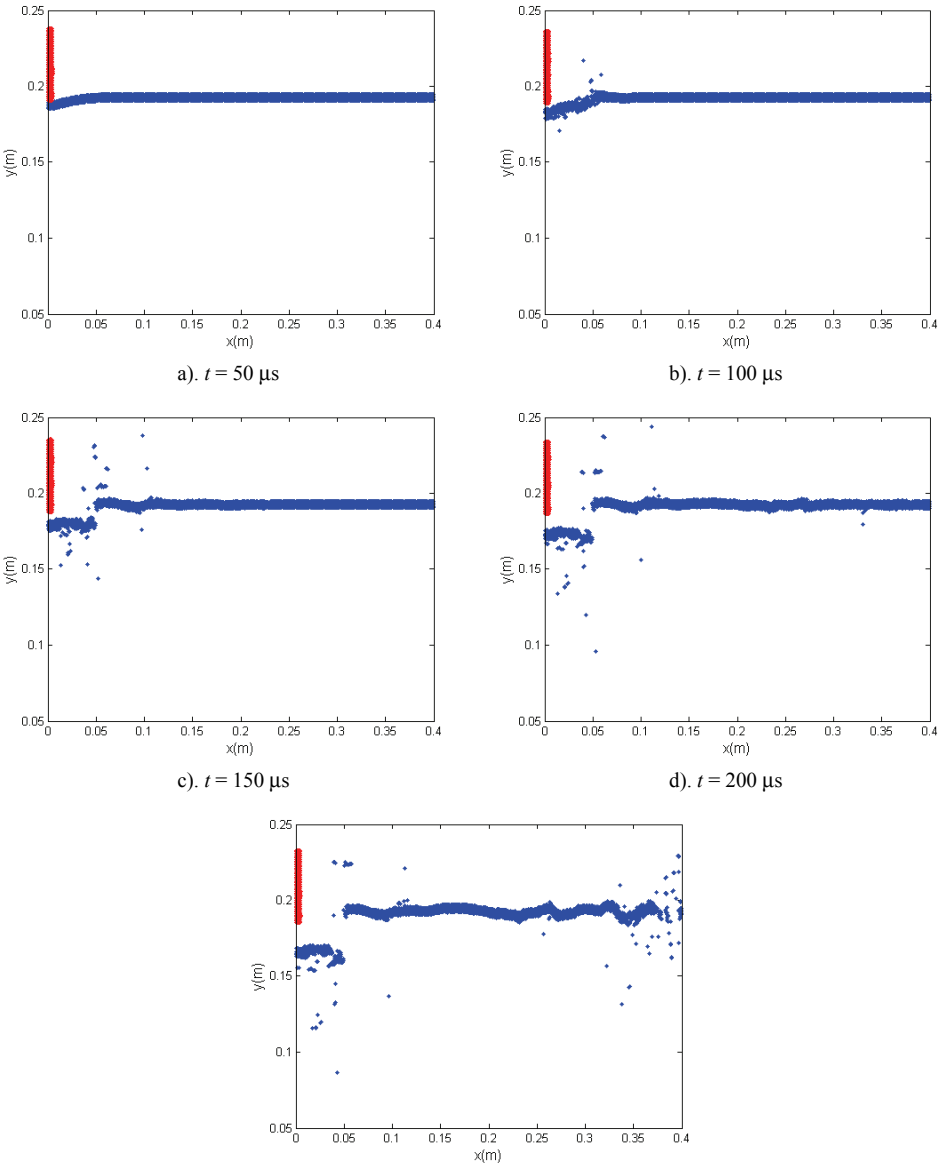

a). t = 50 μs

b). t = 100 μs

c). t = 150 μs

d). t = 200 μs

e). t = 250 μs

Figure 11: Snapshots of a steel cylinder impacting on a glass plate with R = 400 mm at velocity of 200 m/s.

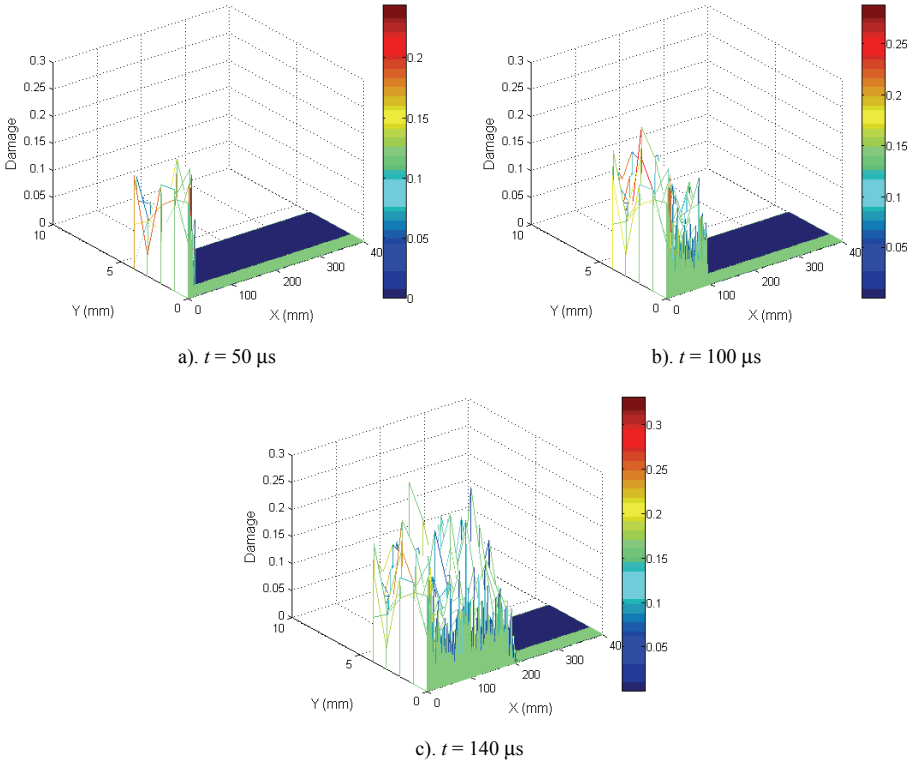

a). $t = 50$ μs

b). $t = 100$ μs

c). $t = 140$ μs

Figure 12: Glass damage contours corresponding to Fig. 11.

Facility in Australia is also acknowledged. The author is grateful to Professor Zhen Chen of the University of Missouri-Columbia for joint discussions.

References

Anderson, C. E.; Bodner, S. R. (1988): Ballistic impact: The status of analytical and numerical modeling. *Int. J. Impact Engg.* Vol. 16, pp. 9–35.

Atluri, S. N. (2004): *The Meshless Method (MLPG) for Domain & BIE Discretizations.* Tech Science Press, 680 pages.

Atluri, S. N.; Han, Z. D.; Rajendran, A. M. (2004): A New Implementation of the Meshless Finite Volume Method, Through the MLPG "Mixed" Approach. *CMES: Computer Modeling in Engineering & Sciences*, Vol. 6, pp. 491-514.

Bardenhagen, S. G.; Kober, E. M. (2004): The Generalized Interpolation Material Point Method. *CMES: Computer Modeling in Engineering & Sciences*, Vol. 5,

pp. 477-496.

Bazant, Z. P.; Chen, E. P. (1997): Scaling of Structural Failure. *Applied Mechanics Reviews*, vol. 50, pp. 593-627.

Belytschko, T.; Krongauz, Y.; Organ, D.; Fleming, M.; Krysl, P. (1996): Meshless Methods: an Overview and Recent Developments. *Comp. Meth. Appl. Mech. Eng.,* vol. 139, pp. 3-48.

Bourne, N. K.; Rosenberg, Z.; Field, J. E. (1995): High-Speed Photography of Compressive Failure Waves in Glasses. *Journal of Applied Physics,* vol. **78**, pp. 3736-3739.

Brar, N. S.; Bless, S.J.; Rosenberg, Z. (1991): Impact-Induced Failure Waves in Glass Bars and Plates. *Applied Physics Letter,* vol. 59, pp. 3396-3398.

Camacho, G.T.; Ortiz, M. (1997): Adaptive Lagrangian modelling of ballistic penetration of metallic targets. *Comput. Methods Appl. Mech. Engrg.* Vol. 142, pp. 269–301.

Chen, Z. (1996): Continuous and Discontinuous Failure Modes. *Journal of Engineering Mechanics*, vol. 122, pp. 80-82.

Chen, Z.; Deng, M.; Chen, E.P. (2001): Rate-dependent transition from tensile damage to discrete fracture in dynamic brittle failure. *Theor. Appl. Fract. Mech.* Vol. 35(3), pp. 229–235.

Chen, Z.; Feng, R.; Xin, X.; Shen, L. (2003): A Computational Model for Impact Failure with Shear-Induced Dilatancy. *International Journal of Numerical Methods in Engineering,* vol. 56, 1979-1997.

Chen, Z.; Hu, W.; Chen, E. P. (2000): Simulation of dynamic failure evolution in brittle solids without using nonlocal terms in the strain–stress space. *CMES: Computer Modeling in Engineering & Sciences*, vol. 1(4), pp. 57–62.

Chen, Z.; Hu, W.; Shen, L.; Xin, X.; Brannon, R. (2002): An Evaluation of the MPM for Simulating Dynamic Failure with Damage Diffusion. *Eng. Fract. Mech.*, vol. 69, pp.1873-1890.

Chen, Z.; Shen, L.; Mai, Y.-W.; Shen, Y. G. (2005): A Bifurcation-Based Decohesion Model for Simulating the Transition from Localization to Decohesion with the MPM. *Zeitschrift für Angewandte Mathematik und Physik (ZAMP)* **56**(5), 908-930.

Chen, Z.; Shen, L.; Kanel, G. I.; Razorenov, S.V., (2001): A Numerical Investigation of Microcracking Diffusion in Sandwiched Glass Plates. *Ceramic Armor Materials by Design*, Edited by McCauley JW et al., Published by The American Ceramic Society, pp. 329-336.

Guo, Y. J., Nairn, J. A. (2006): Three-dimensional dynamics fracture analysis

using the material point method. *CMES: Computer Modeling in Engineering & Sciences*, Vol. 16, pp. 141-156.

Harlow, F.H. (1964): The Particle-in-Cell Computing Method for Fluid Dynamics in Fundamental Methods in Hydrodynamics, *Experimental Arithmetic, High-Speed Computations and Mathematics*, Edited by Alder, B., Fernbach, S. and Rotenberg, M., Academic Press, pp.319-345.

Hu, W.; Chen, Z. (2006): Model-Based Simulation of the Synergistic Effects of Blast and Fragmentation on a Concrete Wall using the MPM. *International Journal of Impact Engineering*, vol. 32, pp. 2066-2096.

Iordache M. M.; Willam, K. (1998): Localized Failure Analysis in Elastoplastic Cosserat Continua. *Computer Methods in Applied Mechanics and Engineering,* vol. 151, pp. 559-586.

Johnson, G. R.; Stryk, R. A.; Beissel, S. R.; Holmquist, T. J. (2001): Conversion of finite elements into meshless particles for penetration computations involving ceramic targets. *Proc., 12th APS Topical Conference on Shock Compression of Condensed Matter*, American Physical Society, pp. 1287–1290.

Kanel, G.I.; Rasorenov, S.V.; Fortov, V.E. (1992): The Failure Waves and Spallations in Homogeneous Brittle Materials. *Shock Compression of Condensed Matter–1991,* Edited by Schmidt, S.C., Dick, R.D., Forbes, J.W., Tasker, D.G., Elsevier, New York, pp. 451-454.

Kanel, G. I.; Razorenov, S. V.; Savinykh, A. S.; Rajendran, A.; Chen, Z. (2005): A study of the failure wave phenomenon in glasses compressed at different levels. *Journal of Applied Physics*, vol. **98**, 113523_1-7.

Klein, P. A.; Foulk, J. W.; Chen, E. P.; Wimmer, S.A.; Gao, H. (2000): *Physics-based Modeling of Brittle Fracture: Cohesive Formulations and the Application of Meshfree Methods. SAND2001-8099*, Sandia National Laboratories, USA.

Le, P., Mai-Duy, N., Tran-Cong, T. Baker, G. (2008): A meshless modeling of dynamic strain localization in quasi-brittle materials using radial basis function networks. *CMES: Computer Modeling in Engineering & Sciences*, Vol. 25, pp. 43-66.

Li, S, and Atluri, S. N. (2008): Topology-optimization of structures based on the MLPG mixed collocation method. *CMES: Computer Modeling in Engineering & Sciences*, Vol. 26, pp. 61-74.

Nairn, J. A. (2003): Material Point Method Calculations with Explicit Cracks. *CMES: Computer Modeling in Engineering & Sciences*, Vol. 4, pp. 649-664.

Ottosen, N. S.; Runesson, K. (1991): Properties of Discontinuous Bifurcation Solutions in Elasto-Plasticity. *International Journal of Solids and Structures,* vol.

27, pp. 401-421.

Schreyer, H. L; Sulsky, D. L; Zhou S. J. (1999): Modeling Material Failure as a Strong Discontinuity with the Material Point Method. *Mechanics of Quasi-Brittle Materials and Structures: A Volume in Honor of Professor Zdenek P. Bazant's 60^{th} Birthday*, (ed. G. Pijaudier-Cabot, et al.), Hermes Science Publications, Paris, pp. 307-329.

Shen, L.; Liu, Y.; Chen, Z. (2001): Bifurcation Analysis of Steel and Concrete with Rate-Dependent Properties Part Two: Bifurcation Analyses and Demonstrations. *Advances in Structural Engineering*, vol. 4, pp. 225-232.

Shen, L.; Chen, Z. (2005a): A Multi-Scale Simulation of Tungsten Film Delamination from Silicon Substrate. *International Journal of Solids and Structures,* vol. **42**(18-19), pp. 5036-5056.

Shen, L.; Chen, Z. (2005b): A Silent Boundary Scheme with the Material Point Method for Dynamic Analyses. *CMES: Computer Modeling in Engineering & Sciences* vol. **7**(3), pp. 305-320.

Sulsky, D.; Chen, Z.; Schreyer, H. L. (1994): A Particle Method for History-Dependent Materials. *Comp. Meth. Appl. Mech. Eng.,* vol. 118, pp. 179-196.

Sulsky, D.; Zhou, S. J.; Schreyer, H. L. (1995): Application of a Particle-in-Cell Method to Solid Mechanics. *Computer Physics Communications,* vol. 87, pp. 236-252.

Taylor, L. M.; Chen, E. P.; Kuszmaul, J.S. (1986): Microcrack-induced damage accumulation in brittle rock under dynamic loading. *Comput. Methods Appl. Mech. Eng.* vol. 55, pp. 301–320.

Wallstedt, P. C., Guilkey, J. F. (2007): Improved velocity projection for the material point method. *CMES: Computer Modeling in Engineering & Sciences*, Vol. 19, pp. 223-232.

Wei, J.; Dharani, L.R. (2005): Fracture Mechanics of Laminated Glass Subjected to Blast Loading. *Theoretical and Applied Fracture Mechanics*, vol. 44, pp. 157-167.

Xu, X. P.; Needleman, A. (1994): Numerical Simulations of Fast Crack Growth in Brittle Solids. *Journal of the Mechanics and Physics of Solids,* vol. 42, pp. 1397-1434.

Zhang, Y. Y., Chen, L. (2008): A simplified meshless method for dynamic crack growth. *CMES: Computer Modeling in Engineering & Sciences*, Vol. 31, pp. 189-200.

Zukas, J. (1990): Survey of computer codes for impact simulation. *High Velocity Impact Dynamics*, Editted by Zukas, J., Wiley, New York, pp.593–714.